Hindawi
Shock and Vibration
Volume 2021, Article ID 1459260, 19 pages
https://doi.org/10.1155/2021/1459260

Research Article

Research on Damage Assessment of Buried Standard and Carbon-Fibre-Reinforced Polymer Petroleum Pipeline Subjected to Shallow Buried Blast Loading in Soil

Ying Cui,[1,2] **Jun Fang**,[1] **Zhan Qu**,[1,2] **Meimei Song**,[1] **and Junhai Zhao**[3]

[1]*School of Mechanical Engineering, Xi'an Shiyou University, Xi'an 710065, China*
[2]*The Key Laboratory of Well Stability and Fluid & Rock Mechanics in Oil and Gas Reservoir of Shaanxi Province, Xi'an Shiyou University, Xi'an 710065, China*
[3]*School of Civil Engineering, Chang'an University, Xi'an 710061, China*

Correspondence should be addressed to Junhai Zhao; zhaojh@chd.edu.cn

Received 19 April 2021; Accepted 6 August 2021; Published 18 August 2021

Academic Editor: Hongyuan Zhou

Buried petroleum pipelines may encounter threats from blast loading due to terrorist attacks, accidental explosions, and artificial blasting during in-progress construction. Carbon-fibre-reinforced polymer (CFRP) is often used for the repair and reinforcement of buried petroleum pipelines. It is meaningful and necessary to distinguish the different responses and establish an effective damage assessment method for standard petroleum pipelines and CFRP-supported petroleum pipelines buried in soil under blast loading. In this study, under fixed end constraints, experimental analysis and numerical simulations were combined to assess the damage of a standard petroleum pipeline and a CFRP petroleum pipeline buried in soil under blast loading. The results showed that, for a scaled distance of 0.19 m/kg$^{1/3}$, plastic deformation occurred on the surfaces of the two pipelines facing the explosive. The antiexplosion performance of the CFRP pipeline was better than that of the standard pipeline, and the CFRP sheets had a positive effect on the protection of the buried petroleum pipeline during the buried blast loading. Furthermore, based on pressure-impulse damage theory and with consideration of the feasibility under real circumstances, two pressure-impulse damage evaluation curves for standard and CFRP pipelines facing explosive loads were established separately based on a new critical ratio of the dent depth and length. Finally, based on the two pressure-impulse damage evaluation curves and the new critical ratio, two pressure-impulse damage criteria for these two buried petroleum pipelines were defined. Moreover, with the two pressure-impulse damage evaluation curves, mathematical formulae for the two different buried petroleum pipelines were established to generate pressure-impulse diagrams. With the established formulae, the damage to the standard buried pipeline and the CFRP pipeline could be evaluated effectively. Damage to other similar standard pipelines or CFRP pipelines buried in soil with different design parameters due to shallow buried blast loading could also be evaluated using this method.

1. Introduction

Petroleum pipelines are energy lifeline systems that are closely related to strategic and economic interests, and their safe operation and maintenance are of great significance to national security and social stability. Most long-distance petroleum pipelines are designed to be buried because buried pipelines are less restricted by terrain and can be kept warm by the soil [1, 2]. However, terrorist attacks, accidental explosions, and artificial blasting during construction in progress have occurred frequently around the world in recent years, posing a challenge to buried petroleum pipeline safety. Blast loading, especially shallow buried blast loading (scaled depth no greater than 0.8 m/kg$^{1/3}$ [3]) has become an objective threat to buried petroleum pipelines. Thus, the dynamic characteristics and explosion resistance performances of buried pipelines should be more of a focus than ever before. Furthermore, it is important to establish a scientific method that can be used to evaluate the safety status after blast loading and to find an effective and

economical way to increase the antiexplosion performances of buried petroleum pipelines. Carbon-fibre-reinforced polymer (CFRP) has a low weight, high strength, and good plasticity, and CFRP is often used to repair structural members such as beams, columns, panels, and walls [4–11]. Additionally, CFRP can improve the impact resistance of a reinforced object and reduce the damage in an oil-gas field [12, 13]. The investigation of the dynamic responses of buried petroleum pipelines and the evaluation of the damage to pipelines with CFRP reinforcement during shallow buried blast loading have important practical significance and theoretical value.

Because of the complexity of explosions in soil and the particularity of pipeline transportation, in recent years, researchers have performed related studies, which mainly focused on two aspects: explosions in soil and responses of buried pipelines.

(1) Studies on propagation characteristics of explosion shock wave in soil medium [14–26]: the propagation of an explosion shock wave in a soil medium involves a damage effect to the target. Therefore, scholars have carried out a large amount of research on the propagation characteristics of explosion shock waves in soil and achieved a series of results. Bjelovuk et al. carried out a series of explosion experiments for the soil surface or in shallow soil, studied the pit forming effect, and established a formula relating the pit forming characteristics and the explosive quantity [14]. Hu et al., based on an explosion experiment, studied the influence of explosions in multilayer ground on the surface expansion damage, and the factors affecting the expansion were studied through an AUTODYN simulation. It was concluded that the buried depth of the explosive was a sensitive factor affecting the surface stress wave and the surface expansion [15]. Karinski et al. analysed the Mach effect of different shapes of rigid structures buried in soil during blast loading with a numerical simulation, and they obtained the pressure distribution around the buried rigid structure [16]. Based on an experimental study and numerical simulations of different depths of an explosion in soil with a buried reinforcement concrete slab, Tan et al. summarized three typical failure modes (conical spalling failure, convex failure, and pit forming failure of the reinforced concrete slab) during blast loading in soil [17]. Song et al. used the common node algorithm, contact algorithm, and Arbitrary Lagrangian–Eulerian (ALE) algorithm to simulate an explosion in soil. The results showed that the equivalent viscoelastic boundary element could effectively and better simulate the infinite foundation energy radiation damping effect in the process of explosion shock wave propagation [18]. Wan et al. carried out experimental and numerical simulation research on the explosion cavity expansion phenomenon of an aluminium fibre explosive in soil, and they obtained the relationship between the explosion cavity radius of the aluminium-fibre explosive and the charge quantity [19]. Through experimental and theoretical analysis, Ren et al. studied the propagation characteristics of an explosion shock wave in loess, and they obtained the wave attenuation index and the variation image of the vibration wave pressure derived from the soil displacement velocity [20]. Through an experiment and numerical simulations, Wang et al. studied the crater shape in wet sand, and they deduced an empirical formula for the crater diameter with different charge quantities and buried depths [21]. Based on the experimental results of an explosion in loess, Wang et al. carried out numerical simulations on the volume change of an explosion cavity in loess, obtained a three-dimensional fit equation, and analysed the influence of the natural density and water content on the volume of the explosion cavity [22]. Based on the superposition of the quasi-static expansion model of spherical charges, Li et al. discussed the error using numerical simulations, and they obtained a formula for the plastic zone radius of a cylindrical charge under the condition of a large length-diameter ratio [23]. Taking an explosion wave as a source, Lu et al. obtained the ground motion parameters of the bedrock and soil layer through on-site testing, and they calculated the corresponding ground motion parameters with the equivalent linearization analysis method. The results showed that the peak value of the acceleration response spectrum was larger than that of the bedrock input [24]. Wang and Gao summarized the commonly used dynamic constitutive models of unsaturated soil and saturated soil as well as the comprehensive elastic-plastic models of soil considering the relaxation effect. Finally, they analysed the application scope and existing problems of various models during blast loading [25]. Ren et al. attributed the responses of soil particles during an underground explosion load to the near-field dynamics, derived the coupling deformation formula of soil particles during an explosion shock wave, and verified their result with a numerical simulation [26].

(2) Studies of dynamic response and influencing factors of common (metal or nonmetal) buried pipelines during blast loading in soil [27–35]: many national standards of buried pipelines in the world have no special clauses or few clauses about the outer blast loading [27–30]. Even though buried pipelines are widely used in transportation, the studies on the dynamic responses and damage statuses of buried pipelines during blast loading are limited. Liang et al. used LS-DYNA to simulate and analyse the dynamic response of a buried gas pipeline during blast loading, and they obtained the relationships between the maximum response (including the velocity and dynamic stress) of the buried pipeline, the charge quantity, and the distance between the explosion centre and the pipeline centre [31]. Gong et al.

carried out a series of experimental studies on buried steel pipes in highly saturated soil during near-field explosions, and they obtained the attenuation law of the peak strain at different positions for different explosion centre distances and buried depths [32]. Abedi et al. regarded an underground pipeline as a beam structure. By establishing a fourth-order, nonhomogeneous partial differential equation and using computer programming, the displacement and the peak particle velocity of the pipeline under the action of underground blast loading were obtained [33]. Zhang et al. studied the buckling failure of buried pipelines for an underground explosion and obtained the buckling failure modes of buried pipelines with different blast loading levels [34]. By using the acceleration time-history function as the input and combining it with a dynamic and static analysis of the pipeline and using the von Mises yield criterion, Shi et al. determined the critical vibration velocity of pipelines during blast loading [35].

Although researchers have conducted many effective explorative studies, studies on how to evaluate the anti-explosion effectiveness of buried pipelines with CFRP sheets subjected to blast loading are still limited [12]. Additionally, due to the widespread use and the importance of buried petroleum pipelines and considering the devastating possible results after an outer blast load is exerted, it is of great importance to investigate the damage effects for buried petroleum pipelines with (or without) CFRP sheets during buried explosion shocks and to establish an effective and convenient damage assessment method.

In this study, with an explosion experiment and numerical simulations, the dynamic responses of a buried standard petroleum pipeline and a buried CFRP petroleum pipeline subjected to blast loading were numerically simulated based on the experimental results of two types of petroleum pipelines during blast loading. Furthermore, based on pressure-impulse damage theory and considering the deformation characteristics of the specimens, effective damage assessment criteria and the corresponding formulae for the two petroleum pipelines were also established. Additionally, the performance of the CFRP sheet was evaluated.

2. Methodology

To evaluate the damage of the buried petroleum pipelines during buried blast loading in soil, two typical specimens, a standard pipeline and a pipeline wrapped with CFRP sheets, were selected and designed. Furthermore, a buried blasting experiment was designed and performed so that the dynamic response and the damage of the petroleum pipelines could be investigated thoroughly.

2.1. Experiment Design and Implementation

2.1.1. Specimen Design. An N80 (which was identified in the American Petroleum Institute Standard) pipeline was selected as the specimen. The outer diameter was 73 mm, the thickness was 5.5 mm, and the length was 750 mm. The basic configuration of the specimens is shown in Figure 1.

To study the different damage statuses and the protection effect of a CFRP sheet wrapped around the pipeline, two pipeline specimens, a standard pipeline and a CFRP pipeline, were designed. The design parameters are shown in Table 1. The basic material properties of the CFRP sheet are shown in Table 2. The cross sections of the two specimens are shown in Figure 2. The basic configuration of the CFRP sheet is shown in Figure 3.

It is known that buried petroleum pipelines are connected by flanges. Since the two specimens were unfit for flange connections, the equipment used to achieve constraints through pipeline specimens, as shown in Figures 4 and 5, was designed. One reaction equipment consisted of a channel steel base, two steel ingot pedestals, and two snap rings. All parts of the reaction equipment were made of steel. Each pipeline specimen was inserted through the snap ring and welded to achieve fixed constraints. The schematic diagram of the equipment used to achieve constraints through pipeline specimens is shown in Figure 4. The equipment dimensions for the experimental conditions are shown in Figure 5.

Based on the Repair of Pressure Equipment and Piping Standard (American National Standards Institute/American Society of Mechanical Engineers PCC-2S-2015), one of the pipeline specimens was chosen to be wrapped with CFRP sheets. The procedure is as follows. After cleaning the pipeline surface with an acetone solution and waiting the solution to completely evaporate, the CFRP sheets were cut based on the dimensions of the pipeline, which was defined between the two snap rings. The premixed carbon-fibre glue was then brushed on the surface of the pipeline specimen, the cut CFRP sheets were stuck on the surface of the pipeline, and the lap length was kept at no less than 100 mm. The procedure is shown in Figure 6.

The lap joint was located on the bottom of the pipeline to keep the lap joint far from the explosion centre. The radial overlap position of the CFRP sheets on the specimen was kept on the back surface of the pipeline to maintain the integration. The axial overlap position of the CFRP sheets on the specimen was kept on more than half-length of the pipeline through the longitudinal direction. After the procedure was complete, the CFRP pipeline specimen was allowed to stand for more than 24 h to ensure that the CFRP sheets stuck to the specimen firmly. The two pipeline specimens and the equipment used to achieve constraints through pipeline specimens are shown in Figure 7.

2.1.2. Experimental Conditions. To investigate the damage and establish an effective assessment method of the buried pipeline with blast loading, an explosion experiment for the standard pipeline and the CFRP pipeline with the same constraint conditions was carried out. The basic test parameters are as follows. TNT was selected as the explosive, and 9.35 kg of TNT was used in the experiments. Since the petroleum pipeline was not buried deeply and shallow buried blast loading usually occurs close to a buried pipeline

Figure 1: N80 specimens.

Table 1: Design parameters of buried pipeline specimens.

Specimen	Length (mm)	Outer diameter of pipeline (mm)	Thickness of pipeline (mm)	Yield strength (MPa)	CFRP
Standard N80	750	73	5.5	551	None
N80 with CFRP	750	73	5.5	551	Two layers

Table 2: Material parameters of carbon-fibre-reinforced polymer (CFRP).

Items	Density (g/mm^3)	Elastic modulus (MPa)	Tensile strength (MPa)	Poisson's ratio	Elongation (%)
Values	1.79×10^{-3}	2.49×10^{5}	3400	0	1.7

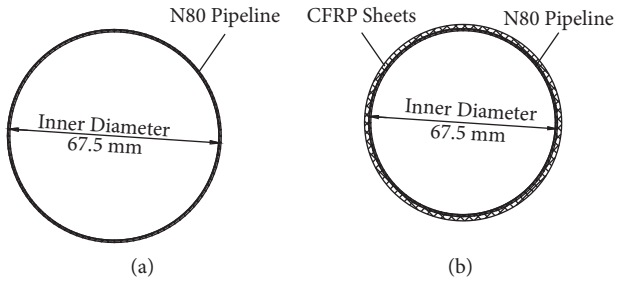

Figure 2: Cross sections of N80 pipeline. (a) Standard N80 pipeline. (b) N80 pipeline with CFRP.

Figure 3: CFRP sheets.

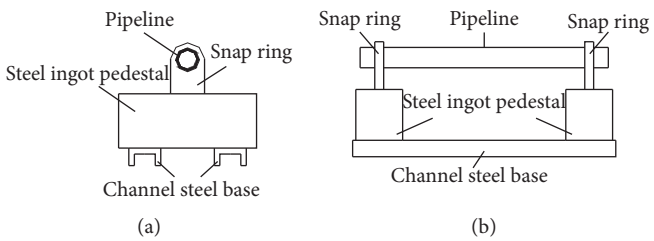

Figure 4: Schematic diagram of the equipment. (a) Side view. (b) Front view.

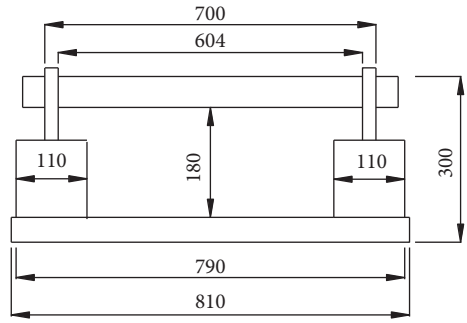

Figure 5: Dimensions of the equipment (units: mm).

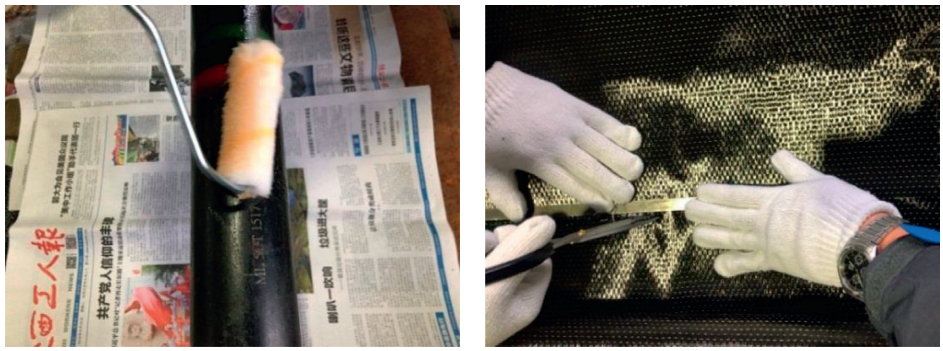

(a) (b)

Figure 6: CFRP sheet wrapping process. (a) Brushing the premixed carbon fibre glue. (b) Cutting the CFRP sheets.

in real circumstances, the vertical distance between the explosion centre and the surfaces of the two pipelines was set as 380 mm. The buried depth of the explosive was 150 mm (the scaled depth was 0.07 m/kg$^{1/3}$). The distance between the explosion centre and the surface of the two pipelines was 440 mm (the scaled distance was 0.19 m/kg$^{1/3}$).

To satisfy the basic test parameters mentioned above, a hole with a depth of 800 mm, a length of 1200 mm, and a width of 900 mm was dug. The hole could accommodate two buried pipeline specimens fixed by the equipment used to achieve constraints through pipeline specimens, and it could satisfy the requirements of the explosion experiment such as the scaled distance and the position of the explosion centre. The schematic diagram is shown in Figure 8. There were two back-filling lines, as shown in Figure 8. The first back-filling line satisfied the buried depth requirement of the explosive, which kept the distance between the explosion centre and the surfaces of the two pipelines at 440 mm. The second back-filling line was the natural ground level. Although the dynamic responses of the pipeline would be influenced by the arrangement of the explosive under the experimental conditions, the main purpose of the site experiment was to examine the final plastic deformation of the two different buried pipeline specimens. The influence of the arrangement of the explosives could be ignored. Thus, there were no testing instruments arranged on the two specimens or buried in the soil.

Photographs of the real experimental field and the specific preparation process are shown in Figure 9. The purpose of the steel bar shown in Figure 9(d) was to calibrate the position of the explosion centre. The hole after the first back-filling and the position of the explosive are shown in Figure 10. The prepared test site is shown in Figure 11.

2.1.3. Experimental Results. The test site after the explosion is shown in Figure 12. A blasting funnel was evident since the explosion occurred at a position close to the natural ground surface. The shallow soil was broken, and it spread outside the original boundary. To examine the damage of the two buried pipeline specimens, excavation was applied carefully until the specimens were visible. The initial photographs of the specimens after excavation are shown in Figure 13 (the left pipeline is the standard pipeline, and the right pipeline is the CFRP pipeline). Significant plastic deformation occurred on the front surfaces of the two pipelines during the blast loading with a scaled distance of 0.19 m/kg$^{1/3}$, and one end of the standard pipeline was broken (Figure 14). Additionally, there were no leaks on the front surface of either specimen.

According to the Risk-Based-Inspection and Assessment Methodology of External Damage for Buried Steel Pipelines Standard (National Standard of the People's Republic of China, GB/T30582-2014), the depth of the dent on the pipeline surface, which is referred to as the maximum deflection value of the bending deformation of the pipeline surface under external loading, was the key parameter used to evaluate the safety of the buried pipelines. The depths of the dents on the two pipeline specimen surfaces were

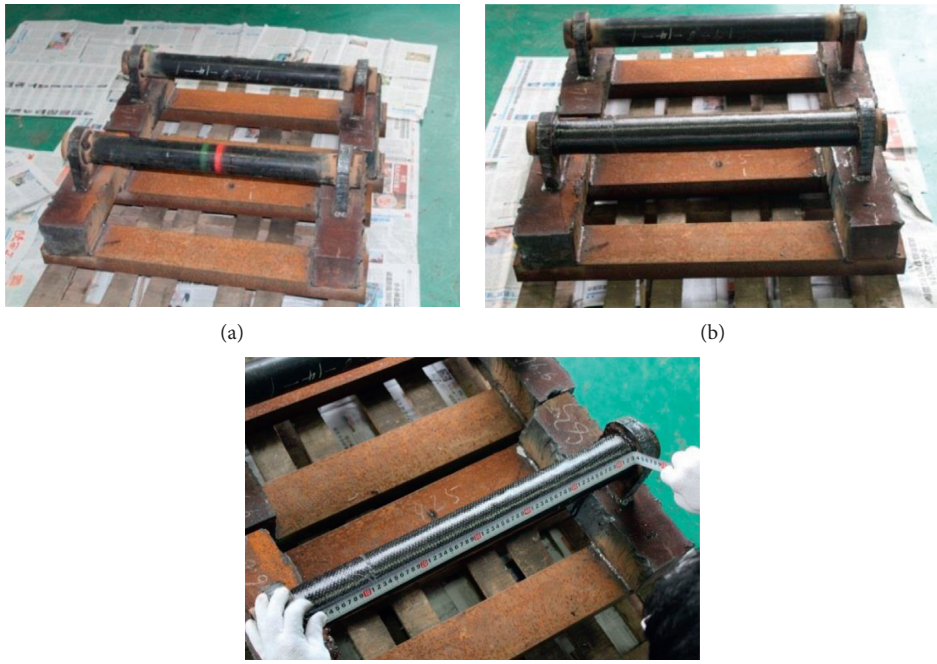

(a) (b)

(c)

Figure 7: Photographs of the specimens and the equipment. (a) Before the CFRP was wrapped. (b) After the CFRP was wrapped (lower pipeline). (c) Pipeline wrapped with CFRP.

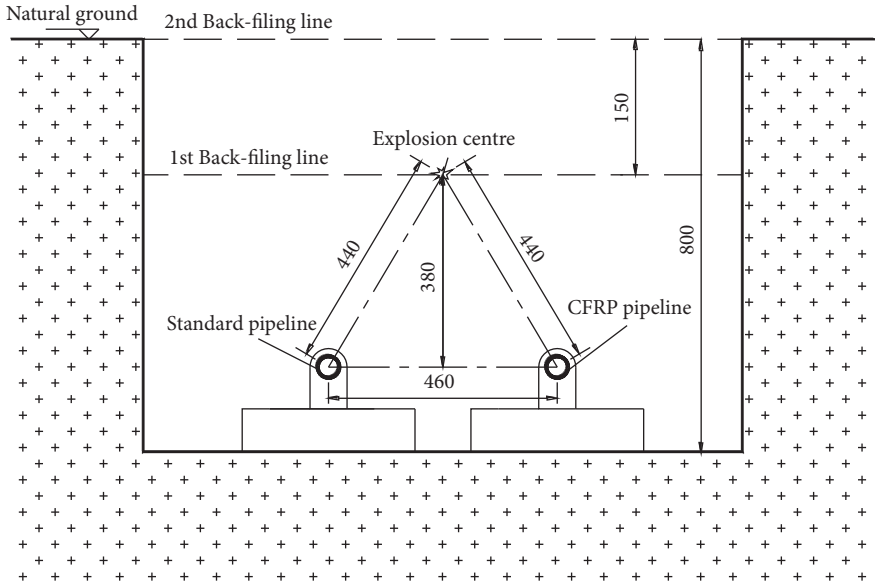

Figure 8: Schematic diagram of the test site (units: mm).

measured separately after excavation. The dent depth of the standard pipeline was 120 mm and that of the CFRP pipeline was 70 mm. Photographs of the macroscopic deformation and the measurement of the two pipeline specimens for the buried blast loading are shown in Figure 15.

2.2. Numerical Simulations. To investigate the antiexplosion performance of the CFRP pipeline and to establish a scientific damage assessment method for the buried pipelines, a numerical model was established in the LS-DYNA software based on the explosion experiment results, and finite element numerical simulations were carried out.

2.3. Constitutive Model of Material. The steel pipelines, air, soil, and explosive were numerically simulated using a SOLID164 element cell, and the CFRP sheets were simulated using a SHELL163 element cell [36, 37]. The corresponding unit system was mm-ms-MPa. The constitutive model of

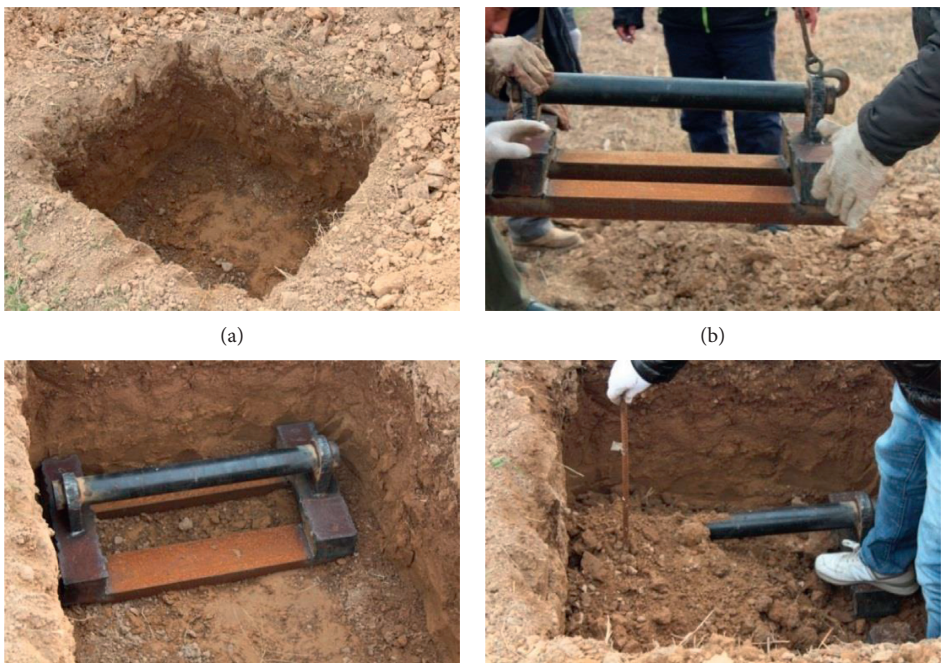

(a) (b) (c) (d)

Figure 9: Test site during preparation. (a) Test hole excavation. (b) Specimen hoisting. (c) Specimen arrangement. (d) Buried depth calibration.

steel pipeline, explosive, and air was performed as described previously [38]. Briefly, material No. 3, material No. 8, and material No. 9 were used to simulate the steel pipeline, the explosive, and the air, respectively, under blast loading. In addition, material No. 5 and material No. 1 were selected as constitutive models of soil and CFRP sheets, respectively, under blast loading. All details are as follows.

(1) *Constitutive Model of Steel Pipeline.*

Material No. 3 (∗MAT_PLASTIC_KINEMATIC) was selected to simulate the dynamic behaviour of the steel pipeline under high strain rates. The corresponding parameters of this constitutive model are shown in Tables 3 and 4.

(2) *Constitutive Model of Soil.*

In the LS-DYNA material selector, material No. 5 (∗MAT_SOIL_AND_FOAM) was selected to simulate the dynamic behaviour of the soil at high strain rates. The corresponding parameters of this constitutive model are shown in Tables 5–8.

(3) *Constitutive Model of CFRP.*

Because the CFRP sheets were not sensitive to the strain rate, material No. 1 (∗MAT_ELASTIC) was selected in the LS-DYNA material selector to simulate the dynamic behaviours of the CFRP sheets before fracture. The corresponding parameters of this constitutive model are shown in Table 9.

(4) *Constitutive Models of Explosive and Air.*

Material No. 8 (∗MAT_HIGH_EXPLOSIVE_BURN) was used to simulate the detonation of the TNT explosive, and material No. 9 (∗MAT_NULL) was used to simulate the air. The parameters of these two constitutive models are shown in Tables 10 and 11.

2.4. Material Equation of State. As described previously [38], an equation of the state was selected to describe the relationship between the volume deformation rate $\Delta V/V$ and the pressure ΔP for the air and the explosives.

2.4.1. Equation of State of Explosive. The ∗EOS_JWL model in LS-DYNA was used to predict the pressure produced in the explosion process, and the predictions were similar to the experimental results. The ∗EOS_JWL model is based on the Jones–Wilkens–Lee equation of the state, which is often used to describe the detonation of explosives [36]:

$$P = A\left(1 - \frac{w}{R_1 V}\right)e^{-R_1 V} + B\left(1 - \frac{w}{R_2 V}\right)e^{-R_2 V} + \frac{wE}{V}, \quad (1)$$

where P is the detonation pressure, V is the relative volume, E is the internal energy per unit volume of the detonation products, and w, A, B, R_1, and R_2 are material constants. The corresponding parameters of the equation of the state of the explosive are shown in Table 12.

2.4.2. Air Equation of State. The ∗EOS_LINEAR_POLYNOMIALequation of the state was used to simulate the properties of the air in the explosion process [39]. The equation of the state can be written as follows:

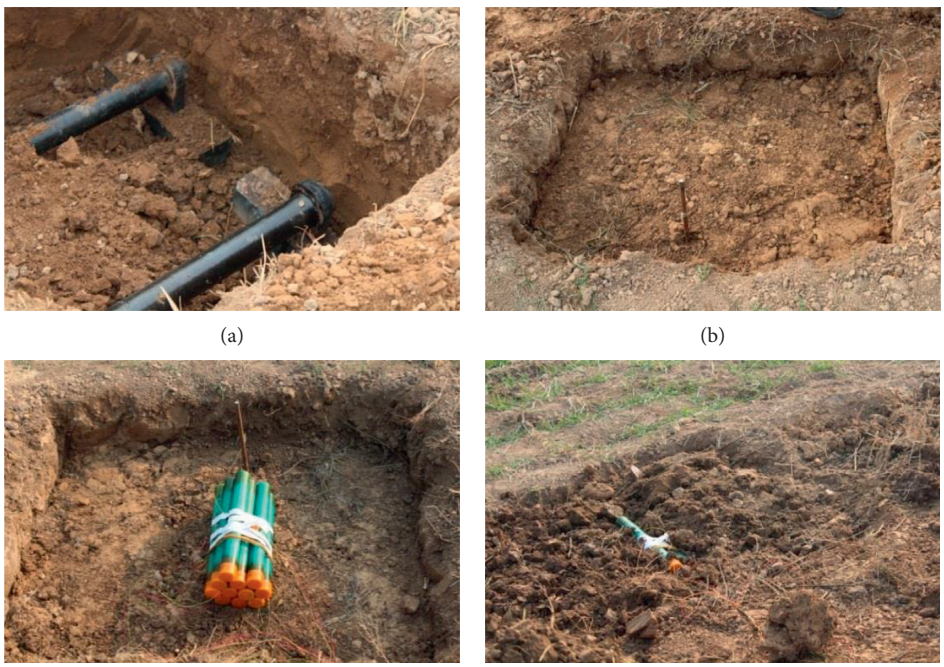

(a) (b) (c) (d)

Figure 10: First back-filling and the position of the explosive. (a) Back-filling. (b) Site after the first back-filling. (c) Explosive arrangement. (d) Buried explosive.

Figure 11: Prepared test site.

Figure 12: Photograph of the test site after explosion.

$$P = C_0 + C_1\mu + C_2\mu^2 + C_3\mu^3 + \left(C_4 + C_5\mu + C_6\mu^2\right)E, \quad (2)$$

where $\mu = (1/V) - 1$, P is the detonation pressure, E is the internal energy per unit volume of the detonation products, and C_0–C_6 are the parameters of the equation of the state.

Figure 13: Initial photograph of specimens after excavation.

Figure 14: Photograph showing one broken end for the standard pipeline.

For air, $C_0 = C_1 = C_2 = C_3 = C_6 = 0$ and $C_4 = C_5 = 0.4$. The corresponding parameters of the equation of the state of air are shown in Table 13.

(a) (b)

Figure 15: Macroscopic deformation of the two pipeline specimens. (a) Standard pipeline. (b) CFRP pipeline.

Table 3: Parameters of *MAT_PLASTIC_KINEMATIC (card1).

Parameters	MID	RO	E	PR	SIGY	ETAN	BETA
Value	1.6	7.83×10^{-3}	2.1×10^{5}	0.3	292.5	2.1×10^{3}	0.0

Table 4: Parameters of *MAT_PLASTIC_KINEMATIC (card2).

Parameters	SRC	SRP	FS	VP
Value	40	5	0.2	0.0

Table 5: Parameters of *MAT_SOIL_AND_FOAM (card1).

Parameters	MID	RO	G	BULK	$A0$	$A1$	$A2$	PC
Value	2	1.73×10^{-3}	63.85	3.0×10^{4}	3.4×10^{-3}	7.033×10^{-2}	0.3	-6.9×10^{-3}

Table 6: Parameters of *MAT_SOIL_AND_FOAM (card2).

Parameters	VCR	REF
Value	0.0	0.0

Table 7: Parameters of *MAT_SOIL_AND_FOAM (card3).

Parameters	EPS1	EPS2	EPS3	EPS4	EPS5	EPS6	EPS7	EPS8
Value	0.0	0.05	0.09	0.11	0.15	0.19	0.21	0.22

Table 8: Parameters of *MAT_SOIL_AND_FOAM (card4).

Parameters	EPS9	EPS10
Value	0.25	0.30

Table 9: Parameters of *MAT_ELASTIC (card1).

Parameters	MID	RO	E	PR	DA	DB	K
Value	3	1.79×10^{-3}	2.49×10^{5}	0.0	0.0	0.0	0.0

Table 10: Parameters of *MAT_HIGH_EXPLOSIVE_BURN (card1).

Parameters	MID	RO	D	PCJ	BETA	K	G	SIGY
Value	4	1.64×10^{-3}	6.93×10^{3}	2.1×10^{4}	0.0	0.0	0.0	0.0

Table 11: Parameters of *MAT_NULL (card1).

Parameters	MID	RO	PC	MU	TEROD	CEROD	YM	PR
Value	5	1.29×10^{-6}	0.0	0.0	0.0	0.0	0.0	0.0

Table 12: Parameters of the equation of the state of the explosive.

Parameters	EOSID	A	B	$R1$	$R2$	OMEG	$E0$	$V0$
Value	4	3.74×10^{5}	3.23×10^{3}	4.15	0.95	0.3	7000	1.0

Table 13: Parameters of the equation of the state of air.

Parameters	EOSID	$C0$	$C1$	$C2$	$C3$	$C4$	$C5$	$C6$	$E0$	$V0$
Value	5	0.0	0.0	0.0	0.0	0.4	0.4	0.0	0.25	1.0

2.5. Finite Element Method (FEM) Model Establishment

2.5.1. Geometric Model and Boundary Conditions. To simulate the real dynamic responses of buried pipelines during shallow buried blast loading, the boundary conditions are determined as follows. The ends of the two pipeline specimens were constrained as fixed ends. Based on previous reports [40, 41] and the conditions of the experiments, the air region and the soil region are defined as follows. The two specimens were surrounded by a rectangular box filled with soil. The box boundaries on the two sides were 300 mm from the outer surface of the pipeline. The box front and back boundaries were 100 mm from the end of the pipeline. The top boundary of the air was 300 mm from the top boundary of the soil, and the bottom boundary of the air was even with the ground. The model geometry is shown in Figure 16.

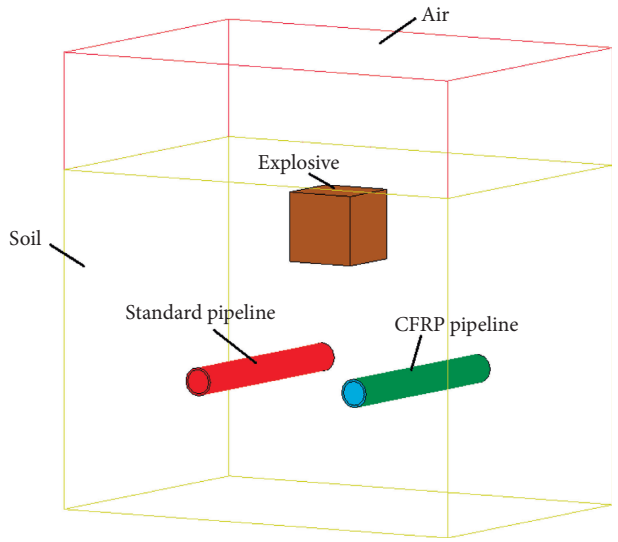

Figure 16: Sketch of the geometric model.

2.5.2. Finite Element Model. Five different materials needed to be simulated. To simulate the flange connection under actual conditions, fixed constraints were applied on all the nodes of the two end sections of the finite element models. With consideration of the properties of different materials and to match closely with the experiment, a SHELL163 element cell was selected to represent the CFRP sheet and a SOLID164 element cell was selected to represent the steel pipeline, soil, explosive, and air. Considering the size effect of the mesh resolution, the efficiency, and the requirement of node sharing [42], the element size was selected to be 20 mm. Thus, the total number of SOLID164 cell units in the finite element model was 138,651, the total number of SHELL163 units in the finite element model was 792, and the total simulation time was set to 30 ms. The boundaries of the numerical model were in accordance with the geometric model. To simulate infinite boundary conditions to represent a real pipeline, each outer surface of the finite element model was defined with nonreflective boundary conditions. The finite element model is shown in Figure 17.

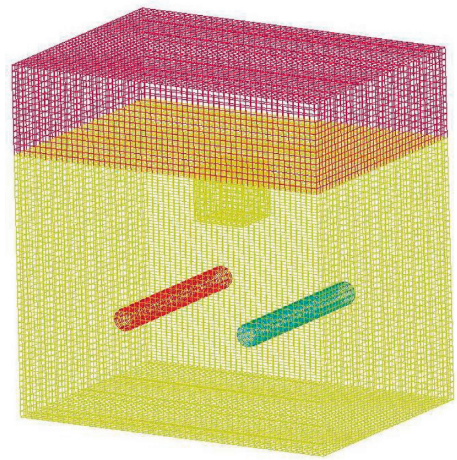

Figure 17: Sketch of the finite element method (FEM) model.

2.6. Numerical Simulation Results. The simulation results are shown in Figure 18. The comparison of Figures 13 and 14 showed that simulation results agreed closely with the experimental results. Bending deformation on the front middle surfaces of the two kinds of pipeline specimens was evident. The deformation of the standard pipeline was greater than that of the CFRP pipeline, which can be seen clearly from another angle in Figure 19. Breakage also occurred on the ends of the standard pipeline, which was somewhat different from the result in the real experiment. However, considering

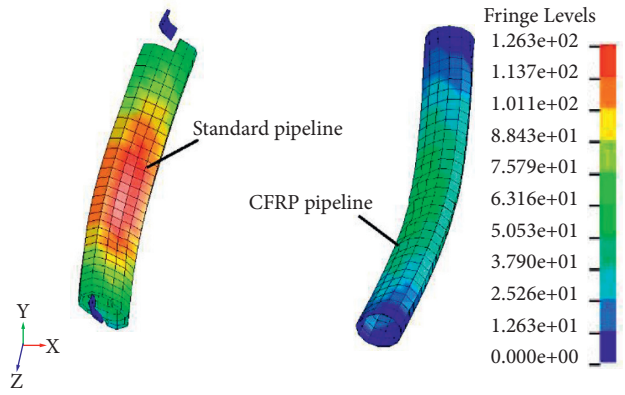

Figure 18: Simulation results for two kinds of pipeline specimens (scaled distance = 0.19 m/kg$^{1/3}$).

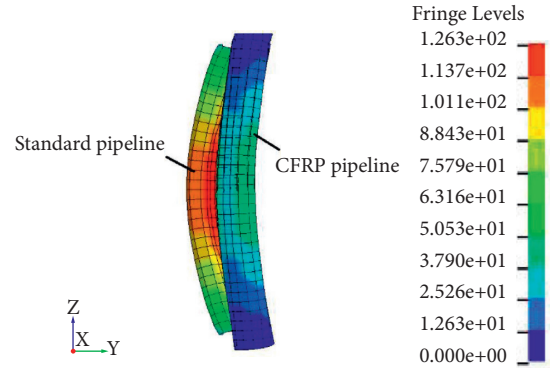

Figure 19: Deformation comparison of the two pipeline specimens (scaled distance = 0.19 m/kg$^{1/3}$).

the differences between the experiment and the simulation and the complicity of the explosion, the simulation results were acceptable, and this simulation approach could be used for further research.

To acquire the deformation amounts of the two kinds of pipeline specimens, the results of the numerical simulations for the standard and CFRP pipelines were plotted, as shown in Figures 20 and 21, respectively.

By comparing the numerical simulation results with the dent depth values of the two pipelines measured in the explosion experiments, the accuracies of the simulations were determined. The dent depths of the two pipelines reached stable values after 2.4 ms in the numerical simulation. As shown in Figure 20, the simulated dent depth of the standard pipeline was 126.32 mm, and the experimental value was 120 mm, corresponding to an error of 5.3%. As shown in Figure 21, the simulated dent depth of the CFRP pipeline was 78.11 mm, and the experimental result was 70 mm, corresponding to an error of 11.6%. The two errors were less than 15%. The comparison of Figures 15 and 18 shows that the deformation shapes of the pipelines in the simulation were in good agreement with those in the experiments, except for the broken ends of the standard pipeline specimen. The reasons for the errors and the differences between the simulation and experimental results are as follows. First, there were differences in the explosion environments. The conditions were ideal in the numerical simulations, but the explosion experiment was affected by factors such as the site conditions (i.e., the influence of the impurities in the soil, the compactness of the back-filling conditions, and deviations from ideal adiabatic conditions) and the measurement accuracy of the dent depth values of the pipelines. Second, there were differences in the constraint conditions. To implement the fixed constraints of the pipelines, a weld joint was used in the explosion experiments, but due to the confinement by the snap ring dimensions of the equipment used to achieve constraints through pipeline specimens, the weld position was only located on the edge (connected to the pipeline directly) of the snap ring. In the simulations, the fixed constraints of the two specimens were fully implemented by confining the nodes of the pipeline end sections. Based on the error, the

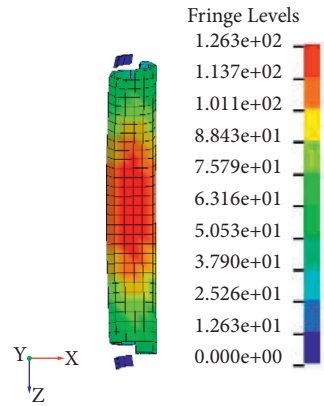

Figure 20: Result of simulation for standard pipeline (scaled distance = 0.19 m/kg$^{1/3}$).

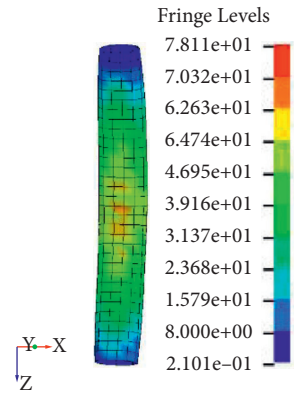

Figure 21: Simulation result for CFRP pipeline (scaled distance = 0.19 m/kg$^{1/3}$).

differences between the experimental and simulation conditions, such as the constraint conditions, the soil conditions, and the compactness of the backfilling, were acceptable, and the numerical simulation results for the two kinds of pipelines with the shallow buried blast loading were reasonable. Thus, the numerical model could be used to perform further damage assessment research for the two kinds of pipelines.

3. Analysis and Evaluation

3.1. Deformation of Pipeline Surface. The results of the in situ explosion experiment and the numerical simulations showed that, for the buried blast loading with a scaled distance of 0.19 m/kg$^{1/3}$, the two kinds of specimens were damaged on the surfaces facing the explosive. The shock wave was uniformly exerted on the two specimens by the soil, so global bending deformation occurred for the two pipelines. At the same time, greater local deformation, i.e., dents, appeared on the front middle surfaces of the two kinds of specimens.

The dent depth values of the standard pipeline were greater than those of the CFRP pipeline for the same shallow buried blast loading and constraint conditions. Furthermore, the standard pipeline was broken at its end. This indicated that the CFRP sheets yielded good antiexplosion effects to protect the buried pipeline.

Since the duration of the in situ explosion experiment was short, the numerical method, which was validated by the comparison described above, was used to obtain the typical dynamic parameters of the two different types of pipeline specimens for blast loading. The deformation-time curves of the front and back middle regions of the two pipelines were obtained from the simulations, as shown in Figures 22 and 23. Since the deformation changes of the two specimens mainly occurred from 0 to 5 ms, the curves in Figures 22 and 23 only show the results from the first 5 ms.

Figure 22 shows that, for the standard pipeline, the greatest amounts of deformation for the front middle surface and the back surface both occurred at 2.4 ms. Additionally, the greatest deformation amount for the front middle surface was 126.32 mm, and the greatest deformation amount for the back middle surface was 90.68 mm. The difference between these deformation amounts was 35.64 mm. This meant that the damage to the back of the standard pipeline was less than that to the front of the pipeline because of the soil buffer and the explosion centre distance. Since the propagation of the shock wave was delayed by the surrounding soil, the beginning time of the deformation on both sides, which is shown in Figure 22, was not at the initial moment. Furthermore, the beginning time of the deformation of the back surface was later than that for the front surface.

The deformation characteristics of the CFRP pipeline, such as the moment of greatest deformation and the deformation distributions on the front and back middle surfaces, were similar to those of the standard pipeline, as shown in Figure 23. In addition, the greatest deformation amount for the front middle surface was 78.11 mm, and the greatest deformation amount for the back middle surface was 36.15 mm. The difference between these deformation amounts was 41.96 mm. In contrast, the beginning time of the deformation of the CFRP pipeline was later than that of the standard pipeline. This meant that the CFRP pipeline was protected by the CFRP sheets, and the deformation of the pipeline was delayed. Based on the differences between the front middle surface and the back middle surface shown in Figures 22 and 23, the CFRP sheets clearly decreased the deformation of the front middle and back middle surfaces of the specimen.

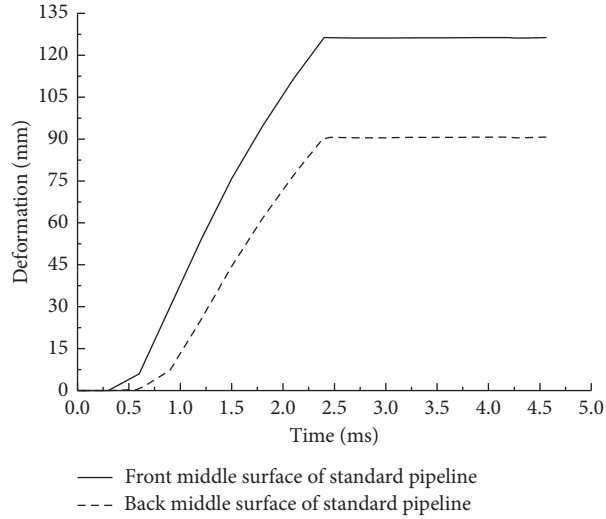

Figure 22: Deformation-time curves at the front and back surfaces of the standard pipeline.

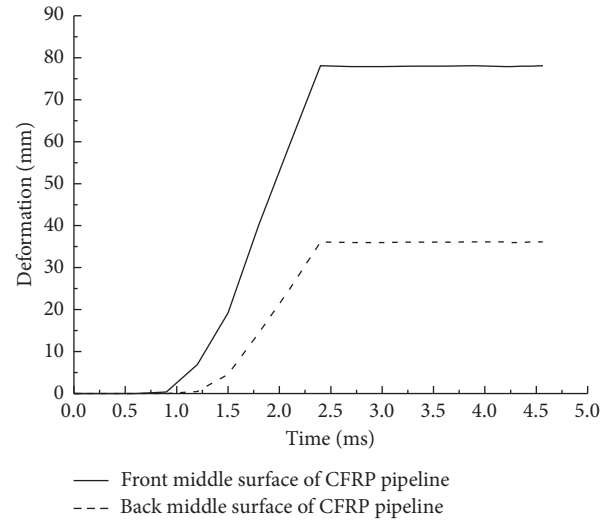

Figure 23: Deformation-time curves at the front and back surfaces of the CFRP pipeline.

To compare the final deformation amounts of the two specimens, the deformation amounts of the front middle and back middle surfaces and the beginning times of the deformation of the pipelines are summarized in Table 14. Based on the data in Table 14, the deformation of the front middle surface of the CFRP pipeline decreased by 38.16% compared to that of the standard pipeline, and the deformation of the back middle surface of the CFRP pipeline decreased by 60.13% compared to that of the standard pipeline. Furthermore, the beginning time of the deformation of the CFRP pipeline was two times later on the front and back middle surfaces compared to that of the standard pipeline. Additionally, the difference between deformation amounts of the front middle and back middle surfaces of the two specimens was similar, and the value for the CFRP

pipeline was 1.43% larger than that of the standard pipeline. All the analysis results showed that the CFRP sheets exhibited good antiexplosion performances during the shallow buried blast loading. Furthermore, due to the protection from the CFRP sheets, the CFRP pipeline deformation was delayed and diminished effectively.

3.2. Propagation Processes of Shock Wave. It is known that the pressure of the shock wave from an explosion is another key factor that affects the damage of a target. The shallow buried explosion caused shock wave propagation both in the air and the soil. The main propagation processes of a shock wave in the soil and the air were determined, as shown in Figure 24.

Figures 24(a)–24(d) show that the pressure values of the shock wave declined rapidly from 82.98 to 7.41 MPa in 2.7 ms. Additionally, the pressure values declined significantly by 88.5% from 0.3 to 1.2 ms. This meant that the shallow buried explosion released energy quickly, and the early response of the object had to be focused on. Deformation of the two pipelines was evident, as shown in Figures 24(b) and 24(c). Furthermore, because the propagation velocity of the shock wave was different in the air and the soil, the shapes of the shock waves were also different, and there was a projectile effect on the boundary between the air and soil that was consistent with the experimental results. Diffraction occurred for the two specimens after the shock wave surrounded them, as shown in Figures 24(c) and 24(d). All the analysis results showed that the shallow buried explosion would result in damage to the buried object and the object near the boundary between the air and soil.

3.3. Pressure-Time History Curves. To evaluate the dynamic responses of the two pipeline specimens, the pressure-time history curves for the front and back middle surfaces of the two kinds of pipeline specimens were also obtained from the numerical simulation results, as shown in Figures 25 and 26. With 9.35 kg of explosives and a scaled distance of 0.19 m/kg$^{1/3}$, the changes of the pressure-time curves at the two positions for the two kinds of pipeline specimens were relatively consistent except for the peak values of the pressure. According to Figures 25 and 26, the initial points of the curves for the back middle surfaces of the two specimens were later than those of the front middle surfaces because of the shock wave propagation. The pressure-time curves of the two pipelines were characterized by steep rises to peak values within short time spans after the explosion had initiated and then steeply dropped, after which the curves gradually approached zero.

As shown in Figure 25, the peak pressure values of the standard pipeline were 28.47 MPa at the front middle surface and 14.70 MPa at the back middle surface. For the CFRP pipeline in Figure 26, the peak pressure values were 20.95 MPa at the front middle surface and 13.51 MPa at the back middle surface. The comparison of the results showed that the peak pressure values of front middle and back middle surfaces of the CFRP pipeline were lower than those of the standard pipeline. For the front middle surface, the peak pressure values of the CFRP pipeline decreased by 26.41%. For the back middle surface, the peak pressure values of the CFRP pipeline decreased by 8.1%. The CFRP sheets decreased the peak pressure values of the buried pipeline.

As shown in Figures 25 and 26, the periods of positive pressure for the two pipelines were approximately 3.5 ms for the front middle surface. For the back middle surface, the periods of positive pressure were approximately 3.2 ms for the two pipelines. Thus, the response times of the two positions for the different pipelines were very close, which means that the CFRP sheets had little effect on the periods of positive pressure.

Based on this analysis, although damage occurred both at the front and back middle surfaces of the two buried pipelines, the CFRP sheets could effectively decrease the damage to some extent. Thus, the damage assessment of the two pipeline specimens should focus on the deformation of the middle of the pipeline surface facing the explosive.

4. Results and Discussion

4.1. Damage Assessment Criterion. A buried petroleum pipeline is a special industrial unit due to its transport conditions, and shallow buried blast loading is very dangerous to buried petroleum pipelines. Additionally, the damage assessment of a buried petroleum pipeline should be effective and easy to perform. During blast loading, permanent deformation will occur to the object. The usability of a pipeline with permanent deformation is meaningful for actual project applications. According to the national standards of the People's Republic of China Risk-Based-Inspection and Assessment Methodology of External Damage for Buried Steel Pipelines (GB/T30582-2014), a dent (permanent deformation) is acceptable for the safety of a pipeline if it is no larger than 6% of the outer diameter of the pipeline. The dent can be defined as the maximum value of the permanent deformation, which is described in Figure 27, where d represents the depth of the dent and l represents the length of the dent. The relationship between d and l is shown in Figure 27, where l corresponds to half of d. Thus, accurate measurement of the depth of the dent should be ensured.

According to the Risk-Based-Inspection and Assessment Methodology of External Damage for Buried Steel Pipelines Standard (GB/T30582-2014), during blast loading, the allowable value of the permanent deformation of an experimental pipeline with a 73 mm outer diameter is 4.38 mm. Since the damage assessment for a member needs to be executed easily on-site, the membrane strain was adopted, which is defined as follows:

$$\varepsilon = \frac{1}{2} \cdot \left(\frac{d}{l}\right)^2. \tag{3}$$

By comprehensively considering the yield strength of the pipeline specimens (550 MPa) and using equation (3), a new effective parameter, the critical failure dent depth-dent length ratio can be defined as follows:

Table 14: Key items of the two pipeline specimens during blast loading.

Key items	Standard pipeline		CFRP pipeline	
	Front middle surface	Back middle surface	Front middle surface	Back middle surface
Final deformation (mm)	126.32	90.68	78.11	36.15
Beginning time of deformation (ms)	0.3	0.6	0.9	1.2
Deformation difference (mm)	35.64		41.96	

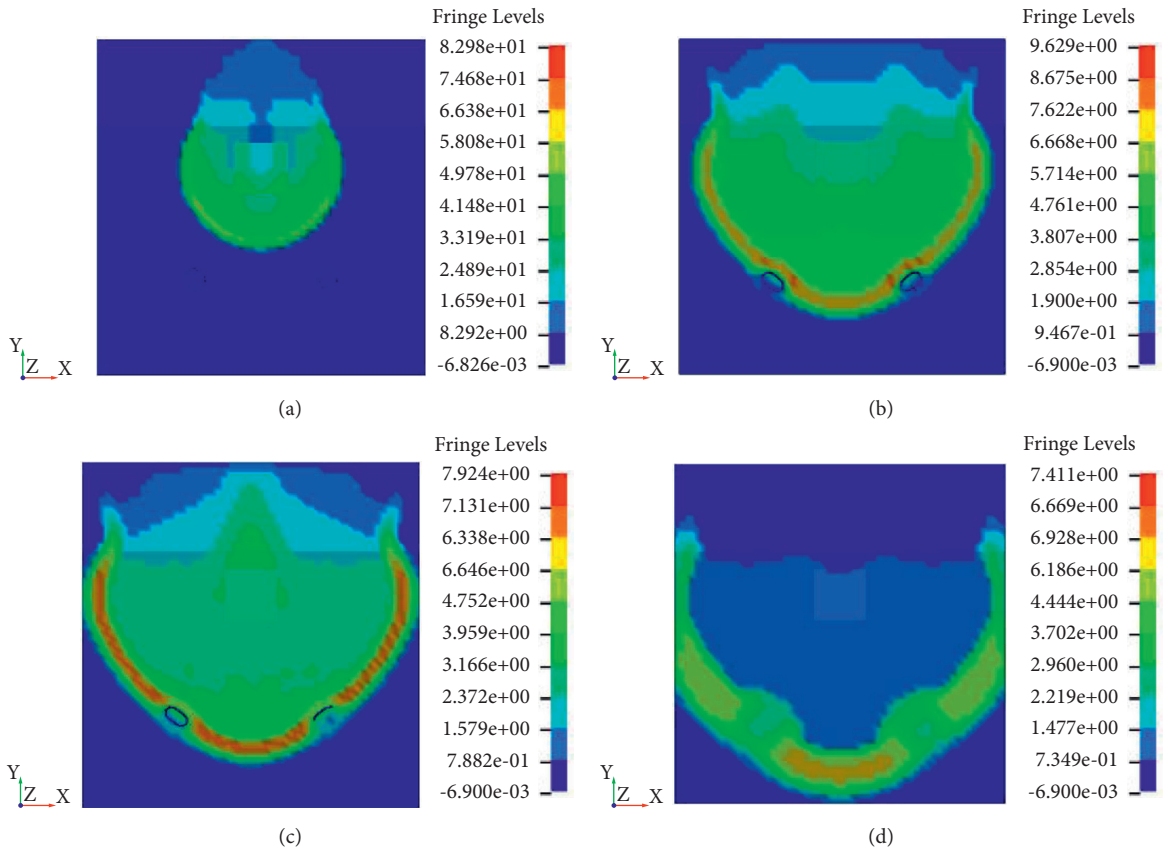

Figure 24: Main propagation processes of the shock wave. (a) Ignition time (0.3 ms). (b) Shock wave touching the pipelines (1.2 ms). (c) Shock wave surrounding the pipeline (1.5 ms). (d) Shock wave touching the bottom boundary (2.7 ms).

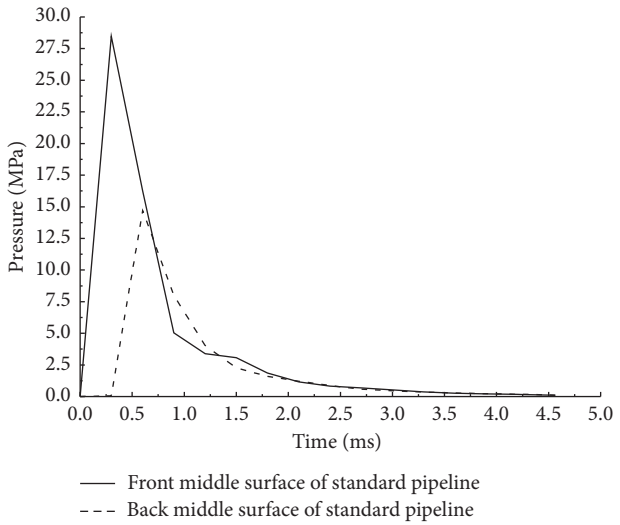

Figure 25: Pressure-time curves at front and back surfaces of standard pipeline.

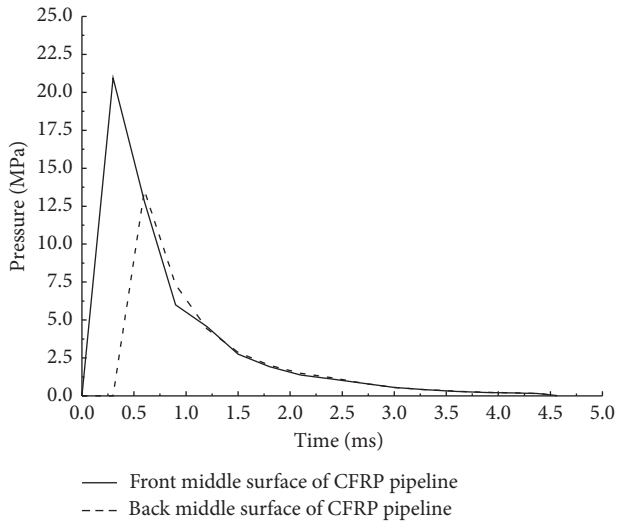

Figure 26: Pressure-time curves at front and back surfaces of CFRP pipeline.

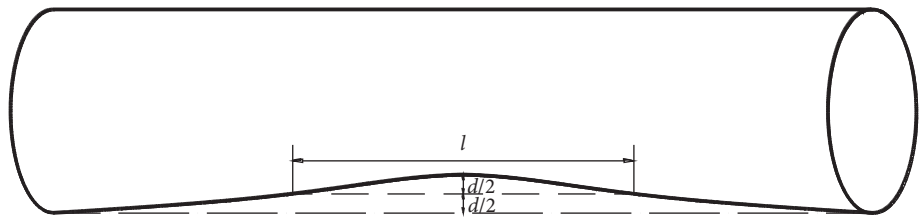

Figure 27: Definition of dent.

$$R_{\text{critical}} = \frac{d}{l} = 0.072. \tag{4}$$

In equation (4), the dent deformation of the pipeline is the maximum plastic displacement. Equation (4) can be described as the damage assessment criterion for buried pipelines, which could be stated simply as follows. If the ratio of the dent depth to the dent length is less than 0.072, the buried pipeline can be determined to be safe. If the ratio of the dent depth to the dent length is greater than 0.072, the buried pipeline can be determined to be unsafe. Since the deformation of the pipeline specimens was caused by blast loading and the pressure and impulse were the two key parameters that mainly determined the damage to a target during blast loading, the pressure-impulse damage assessment criteria for the critical failure dent depth-dent length ratio of two buried pipeline specimens with fixed-end constraints were decided to be established.

4.2. Establishment of Pressure-Impulse Diagram (P-I Curve) for Two Buried Pipelines. The pressure-impulse damage theory was adopted to describe the damage of the two pipelines. In this theory, if the pressure and impulses from the explosion shock waves meet the critical damage criterion of a target, then the target is damaged. The pressure-impulse damage theory can be described as follows [43]:

$$(P - P_{\text{cr}})(I - I_{\text{cr}}) = C, \tag{5}$$

where P_{cr} is a critical value of the pressure that causes a certain amount of damage to the target, I_{cr} is a critical value of the impulse that causes a certain amount of damage to the target, and C is a constant that is related to the characteristics and the damage level of the target.

The established finite element models of the buried standard and CFRP pipelines were adjusted several times to determine the critical pressure and impulse. With the damage assessment criterion defined above as the standard, after each numerical simulation, the displacement-time curve of the element was obtained by selecting the element located in the geometric centre of the pipeline (or the CFRP sheet) surface facing the explosive. The pressure and impulse data obtained from many numerical simulations were plotted in the pressure-impulse (P-I) plane. The critical values of the pressure and impulse were determined from the data, which agreed with the condition of $d = 0.072l$ (equation (4)). The damage diagrams, i.e., the P-I curves, for the standard pipeline and the CFRP pipeline were obtained, as shown in Figures 28 and 29.

The P-I curves established in Figures 28 and 29 show that the P-I plane was divided into two regions. If the P and I data fell to the left of the curve, the ratio of the dent depth to the dent length was less than 0.072 and the deformation of the pipeline was still within the safe range. Thus, the pipeline could be judged to be safe. If the combined data for P and I fell to the right of the curve, the ratio of the dent depth to the dent length was greater than 0.072 and the pipeline could be judged to be unsafe. If the P and I data fell on the curve, corresponding to a critical state, the pipeline could be judged to be unsafe. For example, for the buried explosion experiment and simulation for the standard pipeline, the P and I data ($P = 28.47$ MPa and $I = 18.71$ MPa·ms) fell to the right of the curve shown in Figure 28, and thus, the standard pipeline could be judged to be unsafe for the blast loading in the experiment. Furthermore, for the CFRP pipeline, the P and I data ($P = 20.95$ MPa and $I = 16.22$ MPa·ms) also fell to the right of the curve shown in Figure 29. Thus, the CFRP pipeline was in an unsafe state. Since neither the experiment nor the simulations considered the effect of fluid in the pipelines, the P-I curves for the standard and CFRP pipelines can be used to determine the damage of two types of pipelines without an internal fluid.

To compare the differences between the two P-I curves of the different pipelines, the curves were plotted in the same coordinate system, as shown in Figure 30. The P-I curves of the two pipelines had the same trends, but the curve of the CFRP pipeline was above that of the standard pipeline. The maximum P difference between the two pipelines was close to 86.5% for the condition with the same I value. The results showed that, for the CFRP pipeline, the probability of the P and I data falling to the left of the curve was higher. This meant that the antiexplosion performance of the CFRP pipeline was better than that of the standard pipeline.

4.3. Mathematical Formula for Pressure-Impulse Diagram (P-I Curve). To provide a clear mathematical interpretation for the P-I curves of the two pipelines, the P-I curves in Figures 28 and 29 were fitted with mathematical formulae. Through the analysis of the data, I and P were found to approximately follow a power function relationship. Thus, the P-I curves of the two pipelines could be expressed as follows:

$$P = A \cdot I^{B}, \tag{6}$$

where P is the peak pressure of the blast wave, I is the impulse of the blast wave, and A and B are two real constants that are related to the damage of the pipelines without an

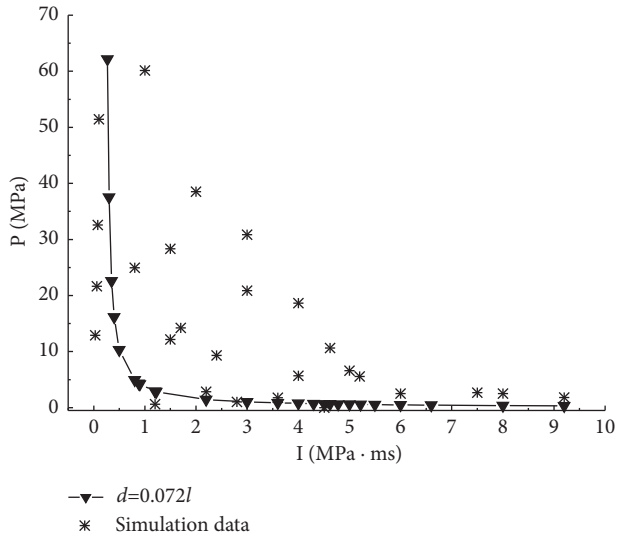

Figure 28: Pressure-impulse (*P-I*) curve of the standard pipeline.

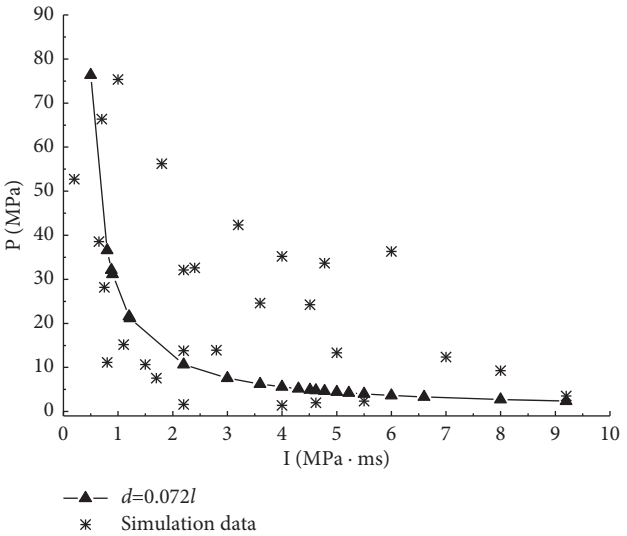

Figure 29: Pressure-impulse (*P-I*) curve of the CFRP pipeline.

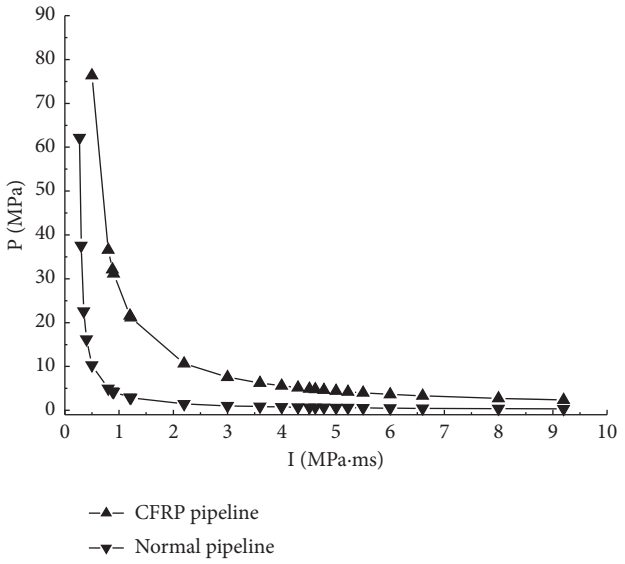

Figure 30: Pressure-impulse (*P-I*) curves of the standard and CFRP pipelines.

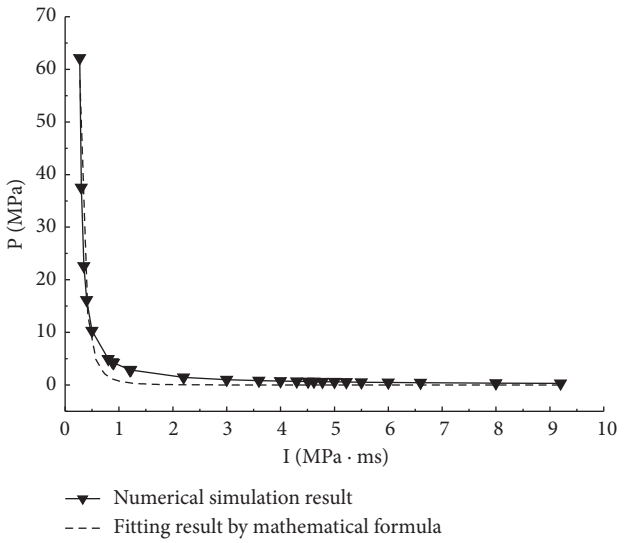

Figure 31: Comparison between the fitted pressure-impulse (*P-I*) curve and the numerical simulation results for the standard pipeline.

internal fluid. The fitting results of equation (6) are shown in Figures 31 and 32.

Figures 31 and 32 show that the curves drawn with the fitting formula were in good agreement with the numerical simulation results. Therefore, by generalizing equation (6), damage assessment criteria for the two kinds of buried petroleum pipelines based on the dent depth-dent length ratio were established. Based on equation (6), the following fitted equation was obtained, and this equation could be used to determine the damage of a standard pipeline without an internal fluid:

$$P = 0.75 \cdot I^{-3.34}, \tag{7}$$

where $A = 0.75$ and $B = -3.34$.

The following equation was similarly determined, and it could be used to determine the damage of the CFRP pipeline without an internal fluid:

$$P = 28.6 \cdot I^{-1.37}, \tag{8}$$

where $A = 28.6$ and $B = -1.37$.

Equations (7) and (8) are suitable for the explosion damage assessment of the buried standard pipeline and the buried CFRP pipeline, respectively, with fixed-end constraints, back-filling conditions, and design parameters presented above (only for these two specimens). Similarly, the fitted pressure-impulse (*P-I*) curves in Figures 31 and 32 could be used to evaluate the safety of these two buried

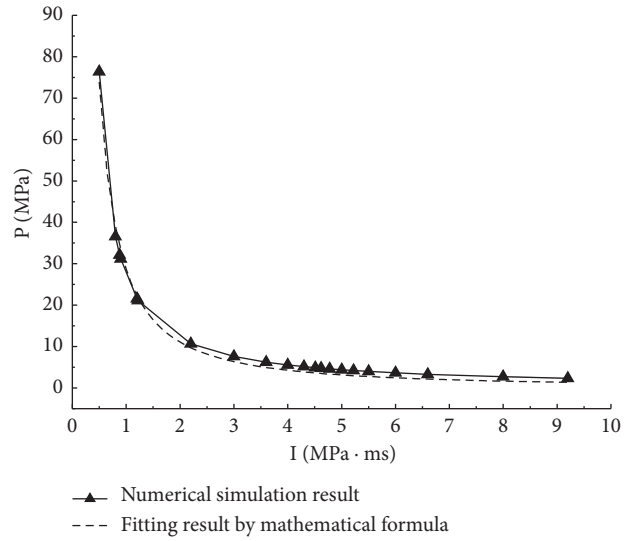

Figure 32: Comparison between the fitted pressure-impulse (*P-I*) curve and numerical simulation results for the CFRP pipeline.

pipelines without an internal fluid and with the design parameters presented above. The corresponding *P-I* curves and formulae for other buried pipelines with different constraints and design parameters (e.g., with different diameters) subjected to shallow buried blast loading could be deduced using the methods summarized in this paper.

5. Conclusions

In this study, the dynamic responses and damage assessment of a buried standard pipeline and a buried CFRP pipeline subjected to buried blast loading were studied using an explosion experiment and numerical simulations. The following conclusions were obtained.

(1) The CFRP sheets had a positive effect on the protection of the buried pipeline during the blast loading after professional wrapping and pasting. The antiexplosion performance of the CFRP pipeline was better than that of the standard pipeline under the conditions described above. The deformation of the buried pipeline and the pressure of the shock wave were decreased effectively. The effect of the CFRP sheets on the decrease in the periods of positive pressure was limited.

(2) The shallow buried explosion was complicated for the shock wave propagation in both air and soil. The objects that were buried or near the surface of the soil were severely damaged by the shallow buried explosion. As an important shallow buried object, buried petroleum pipelines should have preprotection to improve the antiexplosion performance before their installation. Under the same buried blast loading conditions, the blast shock wave caused the most intense damage at the surface facing the explosive. It is important to determine the possible weak points and design CFRP sheet protection reasonably for buried petroleum pipelines.

(3) Confirming an effective and convenient damage assessment method for a buried pipeline after an explosion is important for safety evaluation. An assessment method was determined using the specifications in the national standard and the research described in this paper. The critical ratio between the dent depth and the dent length of a buried pipeline could be adopted as the effective parameter to evaluate the damage during blast loading because this ratio is simple to measure.

(4) Damage assessment criteria for the standard pipeline and the CFRP pipeline were established based on the pressure-impulse damage theory. With the damage assessment criteria, the *P-I* curves and mathematical formulae were derived based on the ratio between the dent depth and the dent length of a pipeline facing the explosive with fixed constraints. Furthermore, the safety performance of other different buried pipelines without an internal fluid and with different design parameters subjected to shallow buried blast loading could be evaluated using the damage assessment criteria.

Data Availability

The data used to support the findings of this study are included within this paper.

Conflicts of Interest

The authors declare that there are no conflicts of interest regarding the publication of this paper.

Acknowledgments

This work was financially supported by the Natural Science Foundation of China (51974255 and 51878056), Natural Science Basic Research Program of Shaanxi Province (2020JM-536 and 2021JQ-605), and State Key Laboratory of Silicate Materials for Architecture Wuhan University of Technology (SYSJJ2019-17).

References

[1] K. Wu, Z. Shao, M. Sharifzadeh, S. Hong, and S. Qin, "Analytical computation of support characteristic curve for circumferential yielding lining in tunnel design," *Journal of Rock Mechanics and Geotechnical Engineering*, vol. 13, pp. 1–9, 2021.

[2] K. Wu, Z. Shao, S. Qin, W. Wei, and Z. Chu, "A critical review on the performance of yielding supports in squeezing tunnels," *Tunnelling and Underground Space Technology*, vol. 115, Article ID 103815, 2021.

[3] D. Ambrosini and B. Luccioni, "Effects of underground explosions on soil and structures," *Underground Space*, vol. 5, no. 4, pp. 324–338, 2020.

[4] A. A. Mutalib, M. H. Mussa, and H. Hao, "Effect of CFRP strengthening properties with anchoring systems on P-I diagrams of RC panels under blast loads," *Construction and Building Materials*, vol. 200, pp. 648–663, 2019.

[5] R. L. Chen, K. Li, Q. Dong et al., "Numerical simulation of dynamic response analysis of reinforced concrete slabs strengthened with CFRP under blast load," *Journal of Railway Science and Engineering*, vol. 17, no. 6, pp. 1517–1527, 2020.

[6] A. Maazoun, S. Matthys, B. Belkassem, D. Lecompte, and J. Vantomme, "Blast response of retrofitted reinforced concrete hollow core slabs under a close distance explosion," *Engineering Structures*, vol. 191, pp. 447–459, 2019.

[7] Y. D. Qu, X. Li, W. L. Liu, W. J. Zhang, and X. Q. Kong, "Numerical analysis of anti-explosion performance of RC beam with initial cracks strengthened with CFRP sheets," *Composites Science and Engineering*, vol. 8, pp. 53–56+26, 2016.

[8] L. Liu, X. Li, Y. Wu, Z. Cheng, and Y. Gao, "Numerical simulation analysis on the antiknock performance of concrete filled steel cylindrical column confined by CFRP," *Steel Construction*, vol. 33, no. 12, pp. 119–124+143, 2018.

[9] B. Kadhom, H. Almansour, and M. Saatcioglu, "Post-blast axial capacity of CFRP strengthened RC columns," *IOP Conference Series: Materials Science and Engineering*, vol. 737, Article ID 012042, 2020.

[10] J. Wan, "Blast response of CFRP-reinforced concrete masonry wall against small stand-off distance explosive charge," *Engineering Mechanics*, vol. 36, no. suppl, pp. 293–297, 2019.

[11] L. Chen, K. Zheng, R. Zhu, and Q. Fang, "Optimization design and dynamic responses of CFRP reinforced masonry infilled wall subjected to vented gas explosion," *Journal of Tianjin University*, vol. 51, no. 5, pp. 547–553, 2018.

[12] M. Mokhtari and A. Alavi Nia, "The application of CFRP to strengthen buried steel pipelines against subsurface explosion," *Soil Dynamics and Earthquake Engineering*, vol. 87, no. 5, pp. 52–62, 2016.

[13] M. Zhang, L. B. Zhu, B. Zhu, H. J. Li, and X. H. Yang, "Current application and prospect of carbon fibre and its composites in oil-gas field," *Hi-tech Fibre and Application*, vol. 42, no. 3, pp. 1–6, 2017.

[14] I. Bjelovuk, S. Jaramaz, P. Elek, D. Micković, and L. Kriĉak, "Modeling of characteristics of a crater emerged from a surface explosion on the soil," *Combustion, Explosion and Shock Waves*, vol. 51, no. 5, pp. 395–400, 2015.

[15] D. Hu, T. Long, C. Liu, G. Yang, and X. Han, "Swelling movement induced by underground explosion of aluminized explosive in multilayered compact material," *International Journal of Rock Mechanics and Mining Sciences*, vol. 71, no. 7, pp. 330–339, 2014.

[16] Y. S. Karinski, V. R. Feldgun, E. Racah, and D. Z. Yankelevsky, "Mach stem due to an underground explosion near a rigid structure buried in soil," *Shock Waves*, vol. 25, no. 1, pp. 63–76, 2015.

[17] Z. Tan, W. Zhang, C. Cho, and X. Han, "Failure mechanisms of concrete slab-soil double-layer structure subjected to underground explosion," *Shock Waves*, vol. 24, no. 5, pp. 545–551, 2014.

[18] J. Song, S. C. Li, and D. F. Zhang, "Numerical simulation of explosion in soil under various arithmetic and boundary conditions," *Blasting*, vol. 31, no. 2, pp. 21–25, 2014.

[19] X. Z. Wan, H. H. Ma, Z. W. Shen, and W. Chen, "Experiment and numerical simulation of explosion cavity in soil by aluminium fibre explosive," *Explosion and Shock Waves*, vol. 36, no. 2, pp. 236–241, 2016.

[20] B. X. Ren, G. Tao, L. N. Xu, H. L. Chen, and C. Q. Pang, "Study on mechanical parameters of vibration wave of the explosion in loess soil," *Science Technology and Engineering*, vol. 16, no. 24, pp. 186–192, 2016.

[21] W. G. Wang, Y. M. Chen, G. Yang, and Y. C. Liu, "Field tests and numerical simulations of blast-induced crater in wet sands," *Chinese Journal of Rock Mechanics and Engineering*, vol. 35, no. 1, pp. 68–75, 2016.

[22] Z. P. Wang, H. C. Li, S. T. Zhou, and B. J. Li, "Numerical simulation of cavity volume rule of explosion in loess," *Blasting*, vol. 33, no. 4, pp. 73–77+126, 2016.

[23] Y. P. Li, Z. Q. Wang, Q. Xu, and X. X. Liang, "Calculation methods for characteristic sizes of blasting cavities induced by finite-length cylindrical charges in soil," *Explosion and Shock Waves*, vol. 39, no. 12, pp. 100–108, 2019.

[24] J. Y. Lu, J. B. Lu, and X. M. Zhou, "Comparative analysis of dynamic responses of soil layers under blast wave," *China Earthquake Engineering Journal*, vol. 41, no. 2, pp. 412–417, 2019.

[25] Y. Wang and K. H. Gao, "Review on calculation methods for interaction between explosion waves in soil and underground structures," *Explosion and Shock Waves*, vol. 35, no. 5, pp. 703–710, 2015.

[26] B. Ren, H. Fan, G. L. Bergel, R. A. Regueiro, X. Lai, and S. Li, "A peridynamics-SPH coupling approach to simulate soil fragmentation induced by shock waves," *Computational Mechanics*, vol. 55, no. 2, pp. 287–302, 2015.

[27] *Guidelines for the Design of Buried Steel Pipe (With Addenda through February 2005)*, American Lifelines Alliance-American Society of Civil Engineers (ASCE), Reston, VA, USA, 2005.

[28] *CAN/CSA-Z662-15, Oil and Gas Pipeline Systems*, Standards council of Canada, Ottawa, Ontario, Canada, 2016.

[29] Y. Liu, Q. S. Feng, X. L. Wang, and H. B. Zhang, "Comparison of Chinese and foreign oil and gas pipeline design standards," *Journal of oil and gas storage and transportation*, vol. 31, no. 1, pp. 45–47+84–85, 2012.

[30] L. He, W. Zhang, D. W. Zhong et al., "Experimental study on dynamic response of buried pipeline subjected to blasting load of tunnel," *Engineering Blasting*, vol. 25, no. 6, pp. 7–13, 2019.

[31] B. Liang, H. Y. Jiang, T. L. Xu, A. L. Yao, and X. Wen, "Impact dynamic response of near-field explosion in buried gas pipeline based on SPH-FEM coupling algorithm," *Acta Petrolei Sinica*, vol. 38, no. 11, pp. 1326–1334, 2017.

[32] X. C. Gong, D. W. Zhong, J. F. Si, and L. He, "Dynamic responses of hollow steel pipes directly buried in high-saturated clay to blast waves," *Explosion and Shock Waves*, vol. 40, no. 2, pp. 13–25, 2020.

[33] A. S. Abedi, N. Hataf, and A. Ghahramani, "Analytical solution of the dynamic response of buried pipelines under blast wave," *International Journal of Rock Mechanics and Mining Sciences*, vol. 88, no. 8, pp. 301–306, 2016.

[34] J. Zhang, L. Zhang, and Z. Liang, "Buckling failure of a buried pipeline subjected to ground explosions," *Process Safety and Environmental Protection*, vol. 114, no. 12, pp. 36–47, 2018.

[35] C. Shi, Q. Zhao, M. Lei, and M. Peng, "Vibration velocity control standard of buried pipeline under blast loading of adjacent tunnel," *Soils and Foundations*, vol. 59, no. 6, pp. 2195–2205, 2019.

[36] J. O. Hallquist, *LS-DYNA Keyword User's Manual*, Livermore Software Technology Corporation (LSTC), Livermore, California, USA, 2007.

[37] S. Q. Shi, J. G. Kang, and M. Wang, *Engineering Applications of ANSYS/LS-DYNA in Explosion and Shock Field*, China Architecture & Building Press, Beijing, China, 2011.

[38] Y. Cui, M. M. Song, Z. Qu, S. S. Sun, and J. H. Zhao, "Research on damage assessment of concrete-filled steel tubular column

subjected to near-field blast loading," *Shock and Vibration*, vol. 2020, Article ID 8883711, 2020.

[39] H. Q. Lu and W. Q. Liu, "Research on numerical simulation of blast wave in air," *Journal of Wuhan University of Technology*, vol. 31, no. 19, pp. 105–108, 2009.

[40] S. B. Li, Z. X. Dong, Y. J. Qi, and J. F. Jiao, "Numerical simulation on decay spread of blasting shock wave in different media," *Journal of Vibration and Shock*, vol. 28, no. 7, pp. 115–117, 2009.

[41] X. Yang, S. Q. Shi, and F. P. Chen, "Forecast and simulation of peak overpressure of TNT explosion shock save in the air," *Blasting*, vol. 25, no. 1, pp. 15–18, 2008.

[42] Y. Shi, Z. Li, and H. Hao, "Mesh size effect in numerical simulation of blast wave propagation and interaction with structures," *Transactions of Tianjin University*, vol. 14, no. 6, pp. 396–402, 2008.

[43] X. Zhou, *Test and Evaluation for Damage Effectiveness of Missile*, National Defense Industry Press, Beijing, China, 2014.